SCIENCE CHINA
Information Sciences

• RESEARCH PAPER •

November 2016, Vol. 59 112213:1–112213:13
doi: 10.1007/s11432-015-5465-9

Output performance optimization for RTD fluxgate sensor based on dynamic permeability

Yanzhang WANG[1,2]*, Shujun WU[1,2], Hao LU[3], Defu CHENG[1,2], Chen CHEN[1,2], Na PANG[1,2], Yunxia WAN[1,2], Zhijian ZHOU[1,2] & Siyu CHEN[1,2]

[1] *College of Instrumentation and Electrical Engineering, Jilin University, Changchun* 130026*, China;*
[2] *Key Laboratory of Geo-Exploration Instrumentation, Ministry of Education, Jilin University, Changchun* 130026*, China;*
[3] *Beijing Aerospace Microsystems Institute, Beijing,* 100094*, China*

Received July 29, 2015; accepted September 2, 2015; published online September 30, 2016

Abstract The output performance of residence times difference (RTD) fluxgate may vary under different driving conditions (driving currents and frequencies) and core materials. To optimize the RTD fluxgate and simplify its design process, an analytical model is employed to select the parameters and identify the effective factors that dominate the performance. The dynamic permeability parameters (P_i), which reflect the changes in the magnetization curve, are mathematically analyzed in detail. The linear variation functions of P_i in different driving conditions are fitted by using the dynamic arctangent hysteresis model. Consequently, the selection of driving conditions and core materials, which are assessed by comparing the experiment and simulation results, has an important role in achieving the optimal output performance of the RTD fluxgate.

Keywords RTD fluxgate, hysteresis loop, analysis of dynamic permeability, simulation, output response

Citation Wang Y Z, Wu S J, Lu H, et al. Output performance optimization for RTD fluxgate sensor based on dynamic permeability. Sci China Inf Sci, 2016, 59(11): 112213, doi: 10.1007/s11432-015-5465-9

1 Introduction

The output performance of a fluxgate is related to magnetic hysteresis because an RTD fluxgate sensor works in the two-way over-saturation state of the magnetic flux density [1–3]. The hysteresis features may demonstrate various behaviors under different driving conditions and core materials [4–7]. As a result, the fluxgate output can only be optimized if suitable ranges of driving conditions and core materials are obtained before designing the fluxgate sensor [8–12].

Diverse approaches have been proposed to optimize the output performance of magnetic sensors [13–18]. One conventional approach analyzes the fluxgate output via the number of experiments, while another approach utilizes a straightforward output expression of the fluxgate according to an ideal mathematical assumption [19–25]. Based on the ideal hysteresis loop for the RTD fluxgate output signal in the time domain, Andò et al. [13] defined the output expression as follows:

$$\Delta T = 2(H^{-1}(-H_c - H_x) - H^{-1}(H_c - H_x)) - T, \tag{1}$$

* Corresponding author (email: jluwyz@126.com)

where ΔT, T, H_x, H_c, and H denote the time difference, excitation field period, target magnetic field, coercive field, and driving magnetic field, respectively [18–23]. Given that the above expression is based on the assumption that the transition of magnetization processes between two stable states is instantaneous, Eq. (1) does not include the permeability of magnetic core materials, which are relevant to the characteristics of the RTD fluxgate [16–17,26]. In other words, the accuracy of the measured magnetic flux density cannot be determined using Eq. (1). Therefore, an accurate model of the RTD fluxgate output response must be developed on the basis of a nonlinear hysteresis model to choose the appropriate driving conditions and core materials for achieving an optimal RTD fluxgate output [17].

Following the working principle of a fluxgate, output response models are tested by using different mathematical approximations for a magnetization curve. For example, Héctor et al. proposed a simple electrical model based on trigonometric approximation for fluxgate harmonic response by comparing different BH curve shapes and driving current waveforms [8]. From this model it was obtained that the maximum nonlinearity deviation of the second harmonic signal magnitude is 0.132%, which is related to the applied external magnetic field. A better method to fit the BH curve was achieved by Zhang et al. who considered the absolute stabilization problem of a class of singular systems with feedback-connected ferromagnetic hysteresis nonlinearities [3]. He established a new boundary condition for the solution of a ferromagnetic hysteresis model by employing the Lyapunov stability approach.

However, there is no any physical parameter of permeability μ included in the two aforementioned models, which leads to an inappropriate selection of the magnetic core for the RTD fluxgate. In addition, in literature [9], Geiler et al. provided a quantitative magnetic hysteresis output model based on the shape of a magnetization curve to analyze the sensitivity and harmonic decomposition of a fluxgate magnetometer. Although the permeability μ in this model is taken as a time-variation value, the maximum error of fitting the hysteresis loop remains as large as 6%. In addition, Andò et al. developed a behavioral model based on a bistable potential energy function to predict the behavior of materials with a sharp hysteresis loop [12,17]. Although the accuracy of the output signal in time domain improved, the RTD fluxgate output response cannot be calculated directly because the parameters involved in this model have no physical meaning.

The aforementioned models do not have the required permeability μ, which is necessary for the RTD fluxgate to detect the target magnetic field via the time difference of the output spiking signal. This manuscript presents: (a) a dynamic arctangent hysteresis model (DAHM) with an accurate permeability μ, which influences the main features of the hysteresis loop, is investigated for RTD fluxgate sensor; (b) an analytical output performance optimization of RTD-fluxgate sensor using DAHM to accurately capture the characteristics of the core materials in working with the random noise, efficiently provide a method to predict dynamic permeability μ parameter when driving field conditions are unknown, and fully consider the effects of driving conditions on the output response; (c) a maximum residual (no more than 5%) of output time difference of RTD fluxgate between the simulation result and the actual measured result, which indicates that the approach of output performance optimization is more suitable for designing an RTD fluxgate sensor.

This manuscript is organized as follows. Section 2 presents the relationship between the dynamic permeability, output response, and extraction procedure of dynamic permeability parameters (P_i), which are analyzed in mathematical forms. Besides, the effects of different driving conditions and core materials on the RTD fluxgate output response are investigated in Section 3 to increase the output stability and sensitivity of the RTD fluxgate as well as improve the output performance of its sensor. The linear variation regulation of P_i in the DAHM is examined by simulating different driving conditions to predict the other parameters when driving field conditions are unknown. The final section provides the output optimization based on the dynamic permeability μ by changing the hysteresis features of the magnetic core model and the driving conditions in PSpice, which provides guidance for designing an RTD fluxgate sensor. Meanwhile, the output optimization approach has been validated by comparing the experiment and simulation results.

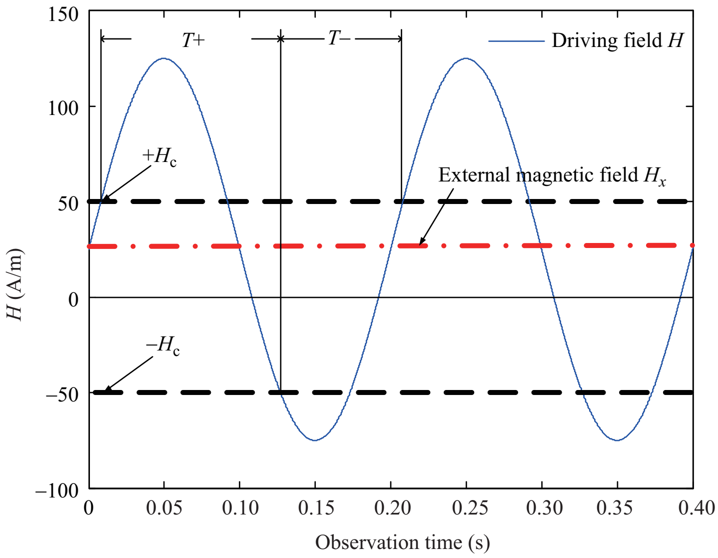

Figure 1 (Color online) Scheme of the time difference generated by the spiking output signals when an external magnetic field exists.

2 Analysis of the effects of dynamic permeability on the RTD fluxgate sensor response

2.1 Working principle of the RTD fluxgate sensor

When the RTD fluxgate is working, the core of the sensor is magnetized by a periodically alternating current in two-way over-saturation. When the excitation field H is higher than the coercive field H_c, the RTD fluxgate magnetic core can generate a spiking output signal. Given that the measured magnetic field is modulated by the RTD fluxgate in the axial direction following the transformer effect, the existing time difference can be used to quantify the target magnetic field (including a weak magnetic field) [17–23]. Figure 1 presents the working principle of the RTD fluxgate.

In Figure 1, the chain line denotes an external target magnetic field along the axial direction of the RTD fluxgate. The sinusoidal signal is the driving field, whereas the dashed line denotes the coercive field. If a target magnetic field exists, then the time difference is not zero (i.e., $\Delta T = T^+ - T^- \neq 0$, otherwise, $\Delta T = T^+ - T^- = 0$) [17–23].

2.2 Effects of dynamic permeability on RTD-fluxgate sensor response

As illustrated in [17], the quality of the output signal is closely related to variations of the dynamic permeability of the magnetic core. Figure 2 illustrates the relationship between the magnetization process and the output response of the RTD fluxgate according to the working principle of the RTD fluxgate sensor.

In Figure 2, the square wave denotes the magnetization process of the magnetic core, while the triangle wave represents the output signal of the RTD fluxgate. The output voltage conversion occurs in the middle state of two-way over-saturation where the value of permeability changes rapidly [17]. Generally, the output signal is not smooth because of noise as shown in Figure 3.

Figure 3 shows how noise affects the output signal of the RTD fluxgate. The pulse denotes the output response. The trigger position of the output signal is varied because of the noise. Several approaches are introduced to increase the slope of the output response and reduce the time difference [18,20,27].

To reduce the effects of noise on the output signal, an effective approach is utilized to select a suitable magnetic core with a large permeability in a specific driving condition [12,17]. The power consumption of the RTD fluxgate is proportional to the driving frequency and current, whereas its sensitivity shows the opposite behavior. To optimize the tradeoff among the power consumption, sensitivity and stability

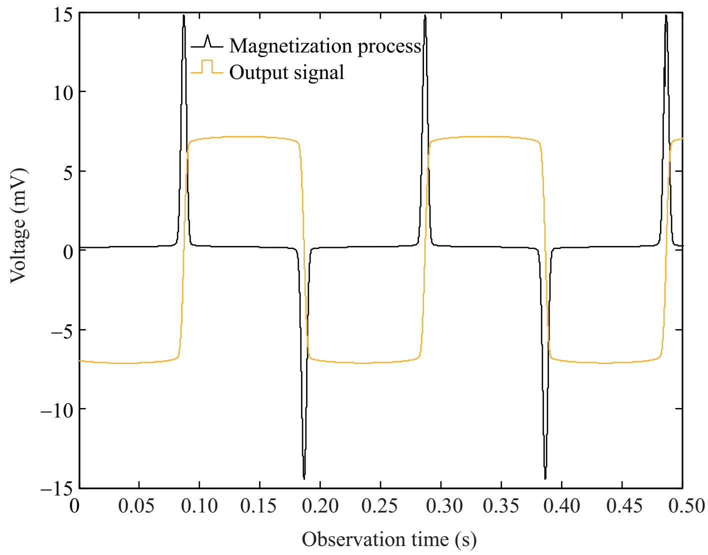

Figure 2 (Color online) Relationship between the magnetization process and output response of the RTD fluxgate.

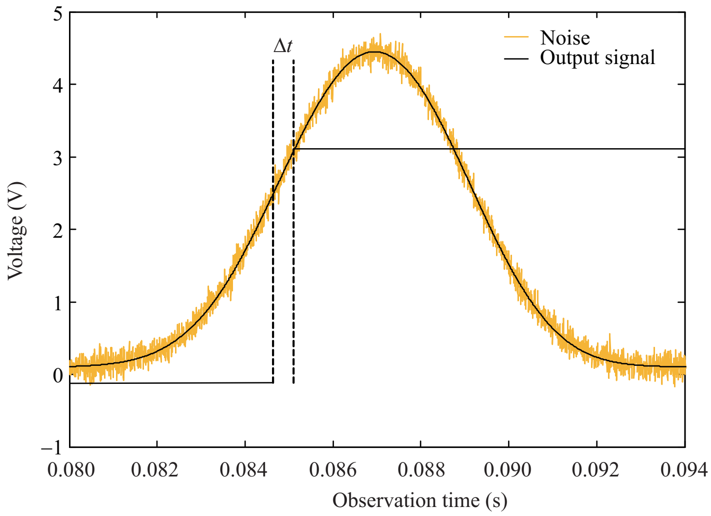

Figure 3 (Color online) Output response of the RTD fluxgate.

of the RTD-fluxgate, the proper driving conditions must be selected to improve the quality of the output signal [9,17–18,20–26].

According to RTD fluxgate detection theory, the large deviation in the output time difference can be caused by a micro variation of dynamic permeability [12,17–18,27]. An output optimization that accurately reflects the variation of dynamic permeability is necessary because the features of magnetic materials are changed under different driving conditions. The solutions to the above questions will be discussed in the following sections.

3 Output optimization of the RTD-fluxgate sensor based on dynamic permeability parameters P_i

3.1 Output response of the RTD fluxgate based on dynamic permeability parameters P_i

The mathematical expression for magnetic flux density in the time domain as presented in the Jiles–Atherton model is difficult to solve and cannot be directly used for the numerical analysis of the RTD fluxgate output. An analytical nonlinear output response model based on DAHM [17] is used instead to calculate the RTD fluxgate output response.

According to Faraday's law, the output signal in the time domain is derived from the magnetic flux density. The output voltage of the secondary coil is expressed as follows [17]:

$$\varepsilon = -\frac{\mathrm{d}B}{\mathrm{d}t} = -\frac{2B_{\mathrm{sat}}}{\pi} \cdot \frac{\mathrm{d}H}{\mathrm{d}t} \cdot \frac{\sum_{i=1}^{n}\left[P_i \cdot (i-1) \cdot (H \pm H_{\mathrm{c}})^{i-2}\right]}{1 + \left\{\sum_{i=1}^{n}\left[P_i \cdot (H \pm H_{\mathrm{c}})^{i-1}\right]\right\}^2}, \tag{2}$$

where B is the core flux density. Given that B denotes the integral of the output signal, its value can be obtained by measuring the induced voltage. B_{sat} denotes the saturation flux density, while H_{c} denotes the coercive field that affects the sensitivity of the RTD fluxgate. These two variables can be provided by the producer. H is the driving field with a known quantity, while P_i denotes the dynamic permeability parameters. B contains the cross section and turn areas of the magnetic core. The response of the RTD fluxgate is typically obtained by measuring the time difference of the output signal, and thus the time difference ΔT can be calculated via numerical calculation to detect a target magnetic field. A close relation is therefore established between dynamic permeability parameters P_i and output response. Such a relation is used to optimize the output of the RTD fluxgate.

3.2 Extraction procedure of dynamic permeability parameters P_i

The actual dynamic permeability μ of a hysteresis loop [17] is described as follows:

$$\mu = \tan(\pi B/2B_{\mathrm{sat}})/(H \pm H_{\mathrm{c}}), \tag{3}$$

where μ reflects the trend of permeability.

The dynamic permeability μ in DAHM is expressed as follows:

$$\mu(H) = \sum_{i=1}^{n} P_i \cdot (H \pm H_{\mathrm{c}})^{i-2}, \tag{4}$$

where P_i denotes the fitting parameters that follow the trend of dynamic permeability μ, while n denotes a fitting accuracy number. Eq. (3) is a mathematical approximation for the dynamic magnetization curve.

To minimize the fitting deviation of Eq. (4), a least squares algorithm is implemented for the extraction of parameters P_i. This algorithm is shown as follows:

$$\delta(P_1, P_2, \ldots, P_n) = \sum_{j=1}^{m}\left[\mu_j - \sum_{i=1}^{n} P_i \cdot (H_j \pm H_{\mathrm{c}})^{i-2}\right]^2, \tag{5}$$

where δ is the residual error, m is the sampling number, μ_j is the dynamic permeability that is quantized from Eq. (3), and H_j is the quantized driving field. To calculate the parameters P_i, the partial differential Eq. (5) of P_i must be obtained as follows:

$$\begin{cases} \frac{\partial\delta(P_1,P_2,\ldots,P_n)}{\partial P_1} = 2 \cdot \sum\limits_{j=1}^{m}\left[\mu_j - \sum\limits_{i=1}^{n} P_i \cdot (H_j \pm H_{\mathrm{c}})^{i-2}\right] \cdot (H_j \pm H_{\mathrm{c}})^{-1} = 0, \\ \frac{\partial\delta(P_1,P_2,\ldots,P_n)}{\partial P_2} = 2 \cdot \sum\limits_{j=1}^{m}\left[\mu_j - \sum\limits_{i=1}^{n} P_i \cdot (H_j \pm H_{\mathrm{c}})^{i-2}\right] \cdot (H_j \pm H_{\mathrm{c}})^{0} = 0, \\ \qquad\qquad\qquad\vdots \\ \frac{\partial\delta(P_1,P_2,\ldots,P_n)}{\partial P_n} = 2 \cdot \sum\limits_{j=1}^{m}\left[\mu_j - \sum\limits_{i=1}^{n} P_i \cdot (H_j \pm H_{\mathrm{c}})^{i-2}\right] \cdot (H_j \pm H_{\mathrm{c}})^{n-2} = 0. \end{cases} \tag{6}$$

Eq. (6) is optimized as follows to find the minimum value of residual error:

$$\begin{cases} \sum\limits_{j=1}^{m}\sum\limits_{i=1}^{n} P_i \cdot (H_j \pm H_{\mathrm{c}})^{i-3} = \sum\limits_{j=1}^{m} \mu_j (H_j \pm H_{\mathrm{c}})^{-1}, \\ \sum\limits_{j=1}^{m}\sum\limits_{i=1}^{n} P_i \cdot (H_j \pm H_{\mathrm{c}})^{i-2} = \sum\limits_{j=1}^{m} \mu_j (H_j \pm H_{\mathrm{c}})^{0}, \\ \qquad \vdots \\ \sum\limits_{j=1}^{m}\sum\limits_{i=1}^{n} P_i \cdot (H_j \pm H_{\mathrm{c}})^{i+n-4} = \sum\limits_{j=1}^{m} \mu_j (H_j \pm H_{\mathrm{c}})^{n-2}. \end{cases} \tag{7}$$

Parameters P_i can be extracted from Eq. (7) by solving one-order polynomial functions in Matlab.

3.3 Analysis of the relation between dynamic permeability parameters P_i and driving conditions

To obtain the corresponding relation between parameters P_i and driving conditions, Eq. (7) is converted as follows:

$$\begin{bmatrix} \sum\limits_{j=1}^{m} (H_j \pm H_{\mathrm{c}})^{1-3} & \sum\limits_{j=1}^{m} (H_j \pm H_{\mathrm{c}})^{1-2} & \cdots & \sum\limits_{j=1}^{m} (H_j \pm H_{\mathrm{c}})^{1+n-4} \\ \sum\limits_{j=1}^{m} (H_j \pm H_{\mathrm{c}})^{2-3} & \sum\limits_{j=1}^{m} (H_j \pm H_{\mathrm{c}})^{2-2} & \cdots & \sum\limits_{j=1}^{m} (H_j \pm H_{\mathrm{c}})^{2+n-4} \\ \vdots & \vdots & \ddots & \vdots \\ \sum\limits_{j=1}^{m} (H_j \pm H_{\mathrm{c}})^{n-3} & \sum\limits_{j=1}^{m} (H_j \pm H_{\mathrm{c}})^{n-2} & \cdots & \sum\limits_{j=1}^{m} (H_j \pm H_{\mathrm{c}})^{n+n-4} \end{bmatrix} \begin{bmatrix} P_1 \\ P_2 \\ \vdots \\ P_n \end{bmatrix} = \begin{bmatrix} \sum\limits_{j=1}^{m} \mu_j (H_j \pm H_{\mathrm{c}})^{1-2} \\ \sum\limits_{j=1}^{m} \mu_j (H_j \pm H_{\mathrm{c}})^{2-2} \\ \vdots \\ \sum\limits_{j=1}^{m} \mu_j (H_j \pm H_{\mathrm{c}})^{n-2} \end{bmatrix}. \tag{8}$$

As shown in Eq. (8), the coercive field H_{c} is fixed when the magnetic core material of the RTD fluxgate is selected. If a solenoid is much longer than its radius and the primary coil of the RTD fluxgate is a single-layer solenoid, then the driving field can be expressed as

$$H = N \cdot I_m \sin(2\pi f t), \tag{9}$$

where N is the number of turns per unit length of the solenoid, I_m is the maximum driving current, and f is the driving frequency. As a result, the parameters P_i are related to the driving conditions (current and frequency). Therefore, if the parameters P_i in different driving conditions are known, then the magnetization curve can be fitted and the output response of the RTD fluxgate sensor can be obtained.

Given that the models of magnetic materials in PSpice allow for the parameters to be controlled accurately and that the core structure of the transformer is similar to the closed RTD fluxgate, the nonlinear magnetic core model in PSpice is utilized as an example for the analysis. The magnetic fields are replaced by a bias DC current that generates an equivalent external magnetic field in the axial direction of the RTD fluxgate according to the detection principle. The simulation circuit of the RTD fluxgate is shown in Figure 4.

As shown in Figure 4, the coupling between the primary and secondary coils is 0.99, while their turns are both 100. The current I and frequency f in driving field $H(I, f)$ are altered by changing the parameters of AC source V_1.

Suitable driving conditions must be selected to design an RTD fluxgate sensor with an excellent performance. As previously discussed, the output response is related to the behaviors of dynamic permeability, while driving field affects the variation in permeability [27]. The parameters P_i in Eq. (4) determine the value of μ. If the corresponding parameters P_i in different driving field conditions are known, then the magnetization curve can be fitted by P_i when the magnetic core material is chosen. In this section, the fitting parameters P_i are determined via simulation in PSpice. The excited output response is generated based on the Jiles–Atherton model to examine the variation regulations of parameters P_i.

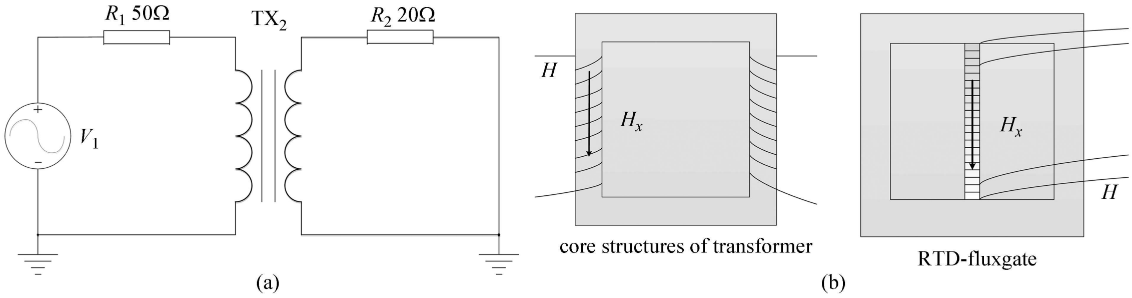

Figure 4 Simulation circuit and core structures. (a) Simulation circuit of the RTD-fluxgate in PSpice and (b) core structures of the transformer and closed RTD fluxgate.

Table 1 Parameters of the magnetic core model in PSpice

	H_c (A/m)	a) H_s (A/m)	b) B_s (T)	c) B_r (T)	d) μ_i (Gs/Oe)	e) μ_m (Gs/Oe)
Value	0.15	32	0.55	0.5	10^5	10^6

a) H_s, b) B_s, c) B_r, d) μ_i, and e) μ_m denote the saturated induction density, saturated magnetic field, residual saturated magnetic inductance strength, initial permeability, and maximum permeability, respectively.

Table 2 Parameters P_i in different driving currents at a 10 Hz frequency

I(mA)	P_5	P_4	P_3	P_2	P_1
35	0.01441	0.05070	−0.05142	0.6906	0.01444
40	0.007746	0.02703	−0.04591	0.6304	0.01994
45	0.004276	0.01479	−0.03860	0.5871	0.02520
50	0.002378	0.008289	−0.03201	0.5533	0.02983

Table 3 Parameters P_i in different driving frequencies at a 40 mA current

F(Hz)	P_5	P_4	P_3	P_2	P_1
5	0.003279	−0.01054	−0.003793	0.6716	−0.7889
10	0.002900	−0.008055	0.01051	0.6471	−0.8901
15	0.002644	−0.006333	0.02293	0.6208	−0.9840
20	0.002454	−0.004620	0.03831	0.5659	−1.038

One magnetic core model corresponds to one magnetic core material when other conditions remain the same. As such, the magnetic core model in Model Editor is implemented for the simulation. Table 1 presents an overview of the model parameters.

To observe the output signal of the secondary coil easily, the two following driving conditions are set: (1) 35–50 mA with a 5 mA interval and (2) 5–20 Hz with a 5 Hz interval. The simulation results of the output signal are analyzed and calculated based on DAHM. In different fitting processes of the magnetization curve using the same magnetic core, the parameters P_i are changed with different driving fields H. The values of corresponding parameters P_i are obtained by using Eq. (4).

Given that the change of μ fits the characteristics of Lorentz function, P_1 in Eq. (4) is used to describe the sharp change of permeability, P_2 is used to describe the bias value of permeability when an external field exists, P_3 is used to describe the dynamic change of permeability, and the high-order terms are mainly used to approximate the details of permeability. The value of n can be selected on the basis of the precision requirement. When $n = 5$, the relative deviations of the two magnetization curves (simulation and measurement) are less than ±3% [17]. When n is increased further, the deviation is not obvious. Therefore, we set n to 5 in this paper. Tables 2 and 3 show the values of P_i in different driving conditions.

As seen from these tables, the parameters P_1, P_2, and P_3 are the linear functions of current and frequency.

When the driving frequency is constant, the linear function is expressed as follows:

$$P_i = a_1 + b_1 \cdot I, \quad i = 1, 2, 3. \tag{10}$$

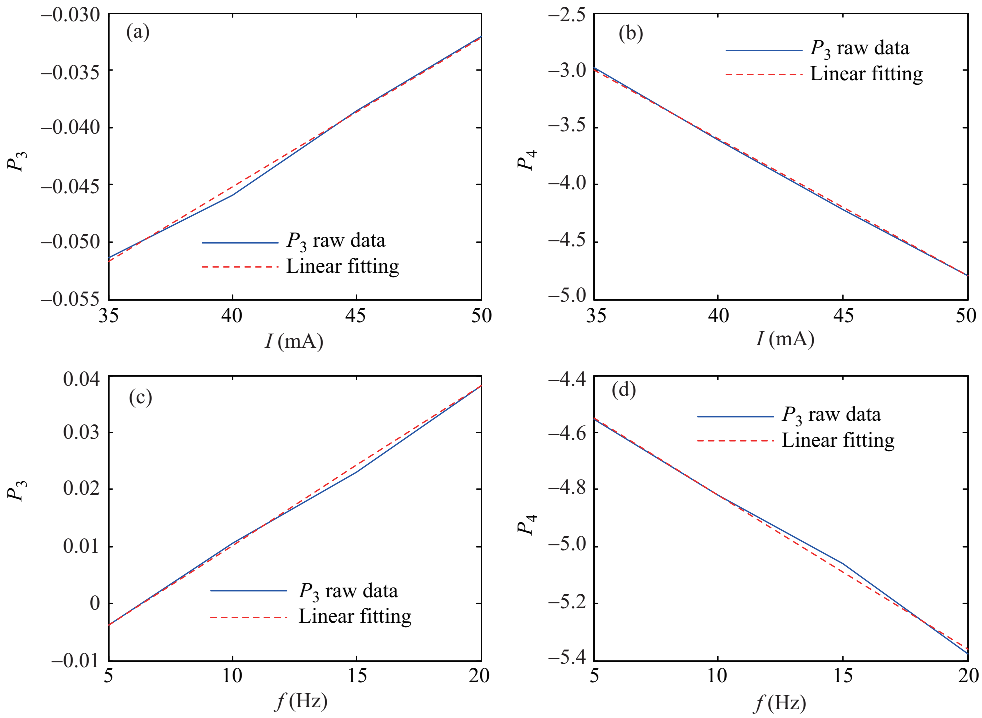

Figure 5 (Color online) Values of parameters P_i and their corresponding fitting curves under different operating conditions. (a) and (b) represent the variations in parameters P_i regular when the frequency is constant and the current varies. (c) and (d) represent the variations in parameters P_i when the current is constant and the frequency varies.

When the driving current is constant, the linear function is expressed as follows:

$$P_i = a_2 + b_2 \cdot f, \quad i = 1, 2, 3. \tag{11}$$

In Eqs. (10) and (11), a_1, b_1, a_2 and b_2 are the fitting parameters.

The logarithms of P_4 and P_5 follow the linear regulation. The fitting curves of P_3 and P_4 are shown in Figure 5. The solid and dashed lines in Figure 5 represent the curve of the calculated values and the fitting curve respectively.

When the driving frequency is constant, the linear function is expressed as follows:

$$\ln(P_i) = a_3 + b_3 \cdot I, \quad i = 4, 5. \tag{12}$$

When the driving current is constant, the linear function is expressed as follows:

$$\ln(P_i) = a_4 + b_4 \cdot f, \quad i = 4, 5. \tag{13}$$

In Eqs. (12) and (13), a_3, b_3, a_4 and b_4 are the fitting parameters. The deviations of parameters P_i between the fitting and actual curves in the simulation are shown in Figure 6.

Figure 6 shows that the relative deviations of parameters P_i in different driving conditions are less than $\pm 5\%$. Given that permeability is affected by driving field, the fitting curve provides a feasible method for efficiently predicting the parameters P_i in an arbitrary driving field. If the features of the magnetic core are known, the characteristics of the RTD fluxgate output response can also be obtained.

3.4 Relation between RTD fluxgate output response and driving conditions

As discussed in the previous section, the dynamic permeability parameters P_i are functions of driving field H. Therefore, the output signal in time domain can be expressed as follows when i= 1, 2, 3:

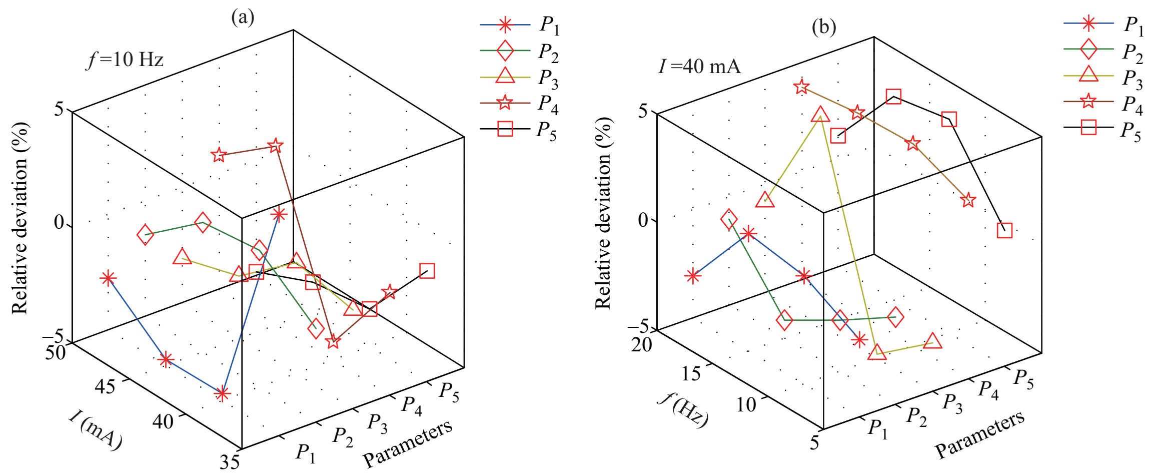

Figure 6 (Color online) Fitting curve deviations of parameters P_i under different conditions. (a) Driving current; (b) driving frequency.

$$
\varepsilon = \begin{cases} \dfrac{2B_{\mathrm{sat}}\mathrm{d}H}{\pi \mathrm{d}t} \cdot \dfrac{\sum_{i=1}^{n}\left[(a_i+b_iI)(i-1)(H\pm H_{\mathrm{c}})^{i-2}\right]}{1+\left\{\sum_{i=1}^{n}\left[(a_i+b_iI)(H\pm H_{\mathrm{c}})^{i-1}\right]\right\}^2}, \\ \dfrac{2B_{\mathrm{sat}}\mathrm{d}H}{\pi \mathrm{d}t} \cdot \dfrac{\sum_{i=1}^{n}\left[(a_i+b_if)(i-1)(H\pm H_{\mathrm{c}})^{i-2}\right]}{1+\left\{\sum_{i=1}^{n}\left[(a_i+b_if)(H\pm H_{\mathrm{c}})^{i-1}\right]\right\}^2}, \end{cases} \quad i=1,2,3, \tag{14}
$$

where a_i and b_i are linear fitting parameters. When $I = 4, 5, \ldots$, the output signal in time domain can be expressed as follows:

$$
\varepsilon = \begin{cases} \dfrac{2B_{\mathrm{sat}}\mathrm{d}H}{\pi \mathrm{d}t} \cdot \dfrac{\sum_{i=1}^{n}\left[\exp(a_i+b_iI)(i-1)(H\pm H_{\mathrm{c}})^{i-2}\right]}{1+\left\{\sum_{i=1}^{n}\left[\exp(a_i+b_iI)(H\pm H_{\mathrm{c}})^{i-1}\right]\right\}^2}, \\ \dfrac{2B_{\mathrm{sat}}\mathrm{d}H}{\pi \mathrm{d}t} \cdot \dfrac{\sum_{i=1}^{n}\left[\exp(a_i+b_if)(i-1)(H\pm H_{\mathrm{c}})^{i-2}\right]}{1+\left\{\sum_{i=1}^{n}\left[\exp(a_i+b_if)(H\pm H_{\mathrm{c}})^{i-1}\right]\right\}^2}, \end{cases} \quad i=4,5\ldots. \tag{15}
$$

In Eqs. (14) and (15), the output signal are connected with the current and frequency. The dynamic permeability parameters P_i in Eq. (2) are replaced by linear functions. The appropriate driving conditions must be selected to achieve a favorable RTD fluxgate output response. In Eqs. (14) and (15), the dynamic permeability parameters P_i are used to dynamically correct the core permeability when the RTD fluxgate is working. The form describes permeability according to the core properties. Based on the output signal and permeability analysis results, a series of simulations and experiments is conducted to achieve output optimization by selecting the driving conditions that are presented in the following section.

4 Output optimization of the RTD fluxgate sensor

4.1 Analysis of the output response based on dynamic permeability in the simulation

The simulation object of the three magnetic core materials is created in Model Editor. The current and turns are set based on the analysis of driving conditions and external magnetic fields. The output time difference of the RTD fluxgate sensor under various situations is obtained by using the output equations. This simulation is performed under different sinusoidal driving fields (current from 20 mA to 80 mA with a 10 mA interval, and frequency from 90 Hz to 300 Hz with a 35 Hz interval) and external magnetic fields (10 A/m). Figure 7(a) shows the time difference of the RTD fluxgate as a function of driving current and frequency.

Figure 7(a) shows that a higher similarity between the driving and coercive fields will increase the sensitivity of the RTD fluxgate [13]. Therefore, the choice of $H_{\mathrm{m}}/H_{\mathrm{c}}$ can increase the sensitivity and

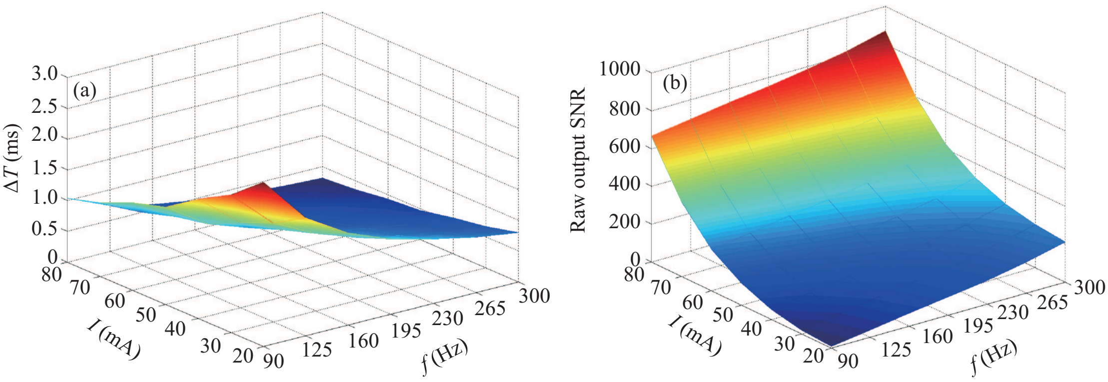

Figure 7 (Color online) Output of the RTD fluxgate in different driving conditions. (a) Output response using the magnetic core model in different driving conditions; (b) output SNR of the RTD fluxgate using the magnetic core model in different driving conditions.

Table 4 Properties of magnetic materials

	2714A annealed	2714A cast	2705A cast
H_{c}(A/m)	0.16	1.6	1.12
μ_{m}(Gs/Oe)	10^6	10^5	10^6

lower the power consumption. Figure 7(a) also shows the time difference of the RTD fluxgate under different driving frequencies. Based on the theoretical analysis of the RTD fluxgate output response as presented in Sections 2 and 3, a proper selection of driving current and frequency can improve the performance of the RTD fluxgate sensor. The current must be reduced and the frequency must be increased to improve stability and achieve a larger output time difference. The driving field has a low limit value because the excitation field must ensure that the RTD fluxgate is working in the two-way over-saturation state of the magnetic flux density. In other words, H must be greater than $H_{\mathrm{c}} + H_x$. Although the reductions in driving current and frequency can benefit the output time difference, these do not positively affect the performance of the sensor because a favorable RTD fluxgate output response not only requires a larger output time difference, but also a high signal–noise ratio (SNR). Figure 7(b) shows the output SNR of the RTD fluxgate in different driving conditions. The output SNR of the RTD fluxgate is proportional to the driving currents and frequencies, but is inversely proportional to the sensitivity as shown in Figure 7(a). Therefore, the proper driving conditions must be selected following an accurate simulation model analysis to optimize the tradeoff between the sensitivity and SNR of the RTD-fluxgate.

4.2 Output response of the RTD fluxgate sensor in the experiment

To verify the simulation results, the output response of the RTD fluxgate sensor is analyzed under the same driving condition and core structure applied in the simulation. The 2714A core is selected because its properties are similar to those of the magnetic core in the simulation. The 2714A and 2705A cast cores are also implemented in the experiment to investigate the output response. The experiment is performed in a magnetic shielding room. Table 4 shows that these three cores primarily differ in terms of their permeability and coercive field. Figure 8 shows the experimental figure.

Two current sources of KEITHLEY 6221 are utilized in experiment to excite the Helmholtz coil for generating a DC target magnetic field and drive the primary coil of the RTD fluxgate. The output responses are acquired by using NI PXI-4495 and FPGA. The output time difference and SNR of the RTD fluxgate sensor under different situations and core materials are shown in Figures 9(a) and (b) respectively.

Different performances of the RTD fluxgate output response can be obtained by utilizing magnetic cores with different properties under the same driving conditions. Figure 9 shows that a low current and frequency can produce a high sensitivity, whereas a high current and frequency can generate a high

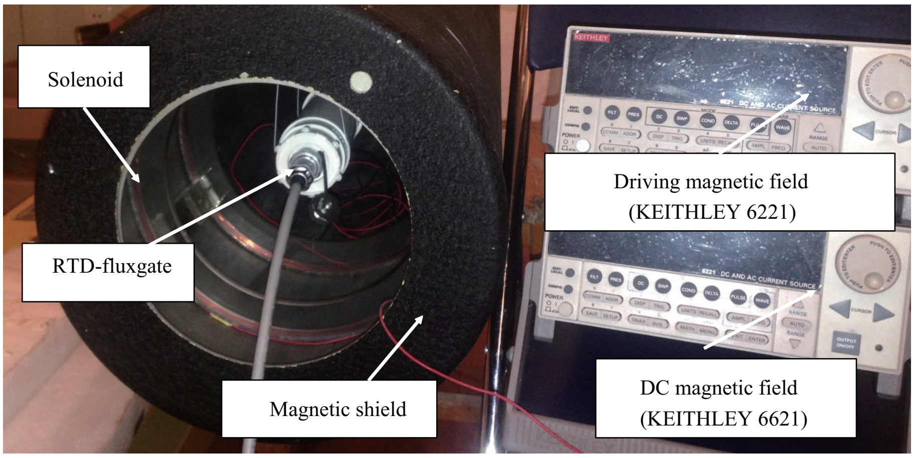

Figure 8 (Color online) Experimental test-bed for testing the magnetic core of the RTD fluxgate sensor adopted in a magnetic shielding room.

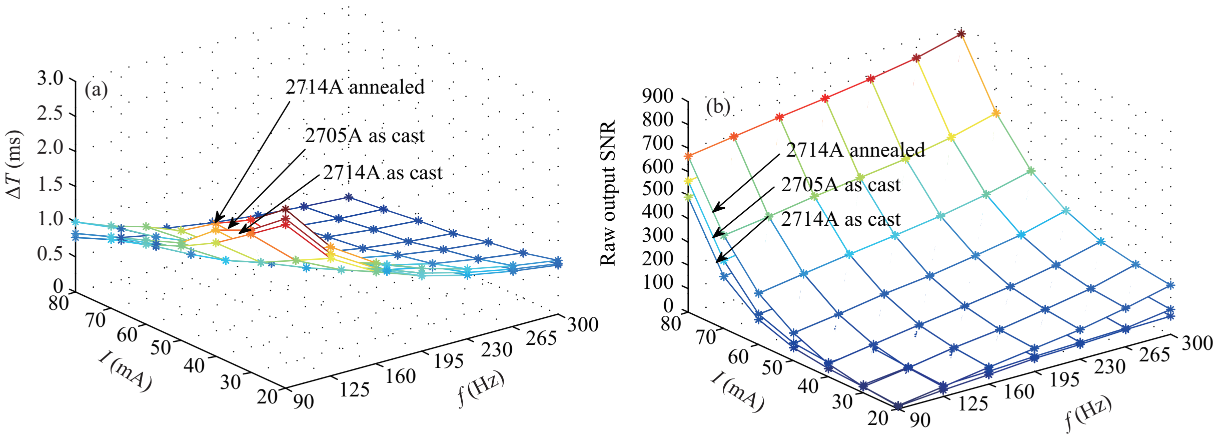

Figure 9 (Color online) Output time difference (a) and SNR (b) of the RTD fluxgate in different driving conditions and core materials.

SNR. The RTD fluxgate sensor that uses the 2714A annealed core material demonstrates a favorable output response and SNR because the 2714A annealed core material has a sharp hysteresis loop and low coercive field. An RTD fluxgate that is designed based on the above properties can produce a spiking output signal and possess a high sensitivity. The driving currents have a greater influence on SNR than driving frequency when a large permeability is observed. To select the proper driving conditions for an RTD fluxgate sensor, different design indicators demand different situations. For example, when the RTD fluxgate properties of ΔT and SNR are selected when $\Delta T > 0.5$ ms and SNR > 200, the optimization of the RTD fluxgate sensor is shown in Figure 10.

Figure 10 shows that under the experiment conditions, the RTD fluxgate sensor demonstrates a favorable output performance in a driving current of 50–80 mA and a driving frequency of 90–160 Hz. These results provide guidance for quickly designing an RTD fluxgate sensor and selecting the appropriate driving conditions and core materials. Three magnetic cores have their own optimization scope of driving conditions. If the database is large enough, the optimization area can be more detailed. Based on the actual requirements, the proper driving conditions of the core can be chosen.

Figure 11 shows the relative deviations of the RTD fluxgate output responses between the measured results (using 2714A annealed core material) and the simulation results (using the approximate simulation model) in the aforementioned situations.

The output responses of the RTD fluxgate are similar to the measured results in different driving conditions. The relative deviations are all less than 5%, which indicates that the simulation method is

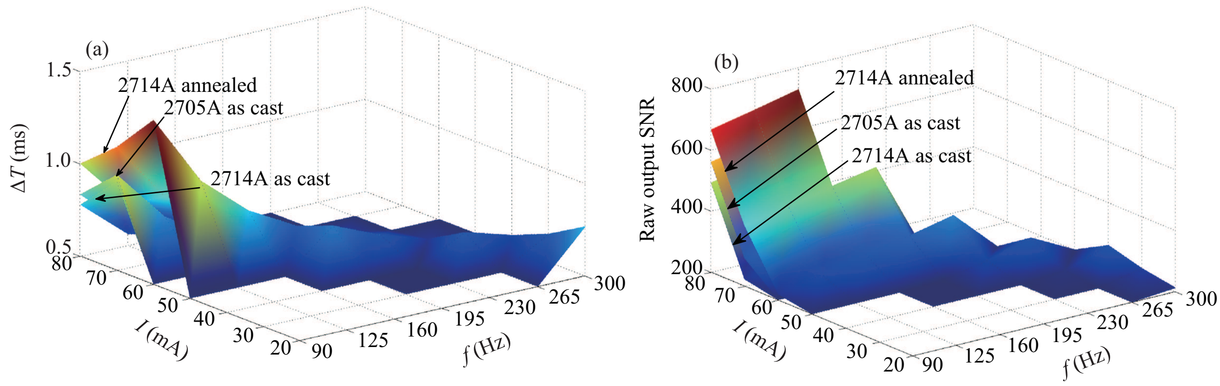

Figure 10 (Color online) Optimization of RTD fluxgate output performance when the sensor properties have different requirements ($\Delta T > 0.5$ ms and SNR > 200) for various driving conditions and core materials. (a) Relation of ΔT; (b) relation of SNR.

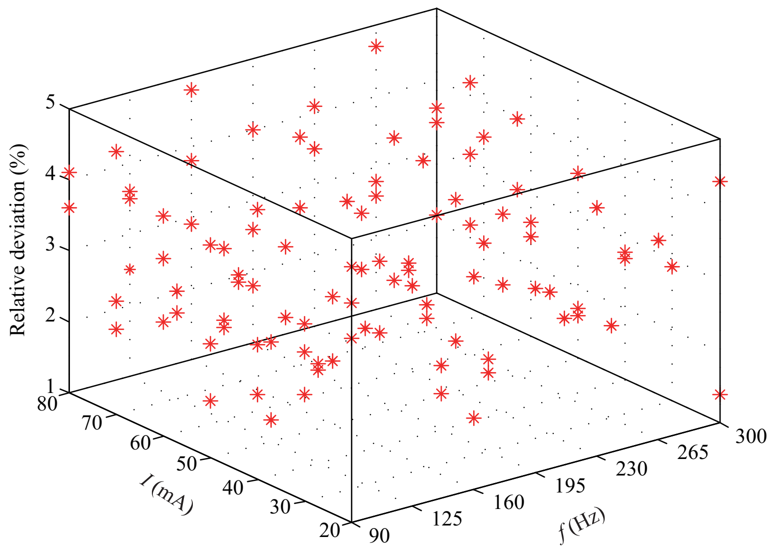

Figure 11 (Color online) Relative deviations of the RTD fluxgate output responses between the measured and simulation results.

suitable for designing the RTD fluxgate sensor. The deviations are mainly caused by the maximum error of permeability when selecting the parameters P_i and the result approximations when using the output model. In addition, the output optimization based on dynamic permeability can accurately capture the characteristics of the magnetic core, conveniently extract the parameters, and provide an approach for selecting the appropriate driving conditions and core materials of the RTD fluxgate sensor.

5 Conclusion

The effects of the dynamic permeability on the output response of the RTD fluxgate were analyzed based on the DAHM. The procedure for extracting the permeability parameters P_i in the DAHM is mathematically analyzed, while the linear variation regulations of parameters P_i were proposed with an error of less than $\pm 5\%$, which is convenient for selecting the appropriate driving conditions of the RTD fluxgate. The output optimization approach was implemented in a simulation and in an experiment using different driving conditions and core materials. The relative time difference ΔT between the simulation and measured results is less than 5%. All in all, the output optimization method can help capture the nonlinearity of the BH curve accurately and select the proper driving conditions and core materials when designing an RTD fluxgate sensor.

Acknowledgements This work was supported by National Natural Science Foundation of China (Grant Nos. 41274183, 40904053), and Science and Technology Development Major Project of Jilin Province (Grant No. 20140203015GX). We also thank the Key Laboratory of Geo-Exploration Instrumentation (Jilin University) Ministry of Education for their additional assistance.

Conflict of interest The authors declare that they have no conflict of interest.

References

1 Andò B, Baglio S, Bulsara A R, et al. RTD fluxgate: a low power nonlinear device to sense weak magnetic fields. IEEE Instrum Meas Mag, 2005, 8: 64–73
2 Primdahl F. The fluxgate magnetometer. J Phys E: Sci Instrum, 1979, 12: 241–253
3 Zhang H G, Wang Y C, Song Z. Absolute stabilization of singular systems with ferromagnetic hysteresis nonlinearity. Sci China Inf Sci, 2013, 56: 078201
4 Sivasubramanian S, Widom A, Srivastava Y. Equivalent circuit and simulations for the landau-khalatnikov model of ferroelectric hysteresis. IEEE Trans Ultrason Ferroelect Freq Control, 2003, 50: 950–957
5 Luo W, Liu S. Fitting the curve of magnetic hysteresis loop of ferromagnetic material of fluxgate. Metallic Funct Mater, 2008, 15: 30–32
6 Ripka P, Butta M, Fan J, et al. Sensitivity and noise of wire-core transverse fluxgate. IEEE Trans Magn, 2010, 46: 654–657
7 Eyal W, Eugene P. Noise investigation of the orthogonal fluxgate employing alternating direct current bias. J Appl Phys, 2011, 109: 07E529
8 Héctor T, Juan C, Mairée R, et al. Analysis of the fluxgate response through a simple spice model. Sensor Actuat, 1999, 75: 1–7
9 Geiler A L, Harris V G, Vittoria C, et al. A quantitative model for the nonlinear response of fluxgate magnetometers. J Appl Phys, 2006, 99: 08B316
10 Andò B, Baglio S, Bulsara A, et al. RTD fluxgate behavioral model for circuit simulation. In: Proceedings of Eurosensors XXIV Conference. Linz: Elsevier Press, 2010. 1288–1291
11 Andò B, Baglio S, Bulsara A R, et al. SPICE simulation of coupled core fluxgate magnetometers. In: Proceedings of Instrumentation and Measurement Technology Conference. Binjiang: IEEE Press, 2011. 1–5
12 Andò B, Baglio S, Bulsara A R, et al. Adaptive modeling of hysteretic magnetometers. IEEE Trans Instrum Meas, 2012, 61: 1361–1367
13 Andò B, Baglio S, Sacco V, et al. Effects of driving mode and optimal material selection on a residence times difference-based fluxgate magnetometer. IEEE Trans Instrum Meas, 2005, 54: 1366–1373
14 Yin C, Jia Z, Ma W C, et al. Modeling and analysis of nano-sized GMRs based on Co, NiFe and Ni materials. Sci China Inf Sci, 2014, 57: 022404
15 Andò B, Ascia A, Baglio S, et al. Towards an optimal readout of a RTD fluxgate magnetometer. Sensor Actuat A Phys, 2008, 142: 73–79
16 Canepa F, Chirafici S, Napolentano M, et al. Nonlinear effects in the ac magnetic susceptibility of selected magnetic materials. J Alloy Compd, 2007, 442: 142–145
17 Wang Y, Wu S, Zhou Z, et al. Research on the dynamic hysteresis loop model of the residence times difference (RTD)-fluxgate. Sensors, 2013, 13: 11539–11552
18 Andò B, Baglio S, Bulsara A R, et al. Investigation on optimal materials selection in RTD-fluxgate design. In: Proceedings of Instrumentation and Measurement Technology Conference. Ottawa: IEEE Press, 2005. 1261–1265
19 Andò B, Baglio S, Bulsara A R, et al. "Residence times difference" fluxgate magnetometers. IEEE Sensor J, 2005, 5: 895–904
20 Bulsara A R, Seberino C, Gammaitoni L, et al. Signal detection via residence-time asymmetry in noisy bistable devices. Phys Rev E, 2003, 67: 016120
21 Andò B, Baglio S, Bulgan A R, et al. A new readout strategy for fluxgate sensor. In: Proceedings of Instrumentation and Measurement Conference. Vail: IEEE Press, 2003. 600–604
22 Nikitin A, Stocks N G, Bulsara A R. Signal detection via residence times statistics: noise-mediated minimization of the measurement error. Phys Rev E, 2003, 68: 036133
23 Andò B, Baglio S, Bulsara A R, et al. "Residence times difference" fluxgate. Measurement, 2005, 38: 89–112
24 Stewart M, Cain M G. Ferroelectric Hysteresis Measurement & Analysis. NPL Report CMMT(A). 1999
25 Lei C, Wang R, Zhou Y, et al. MEMS micro fluxgate sensors with mutual vertical excitation coils and detection coils. Micro Syst Tech, 2009, 15: 969–972
26 Chiesi L, Kejik P, Janossy B, et al. Planar 2D micro-fluxgate sensor. Sens Actuat A Phys, 2000, 82: 174–180
27 Andò B, Baglio S, Pitrone N, et al. Noise effects in RTD fluxgate. IEEE Sensor J, 2005, 4: 935–938